MAGNETIC RESONANCE

Application of the amide proton transfer-weighted imaging and diffusion kurtosis imaging in the study of cervical cancer

Nan Meng[1,2] · Xuejia Wang[3] · Jing Sun[4] · Dongming Han[3] · Xiaoyue Ma[1,2] · Kaiyu Wang[5] · Meiyun Wang[1,2]

Abstract

Objectives To analyze the value of amide proton transfer-weighted imaging (APTWI) and diffusion kurtosis imaging (DKI) in differentiating cervical cancer (CC) pathological type, grade, and stage.

Methods One hundred and twelve women underwent pelvic APTWI and DKI. The magnetization transfer ratio asymmetry (MTRasym, 3.5 ppm), apparent kurtosis coefficient (K_{app}), and non-Gaussian diffusion coefficient (D_{app}) were calculated by histological subtype, grade, and stage. The differences, efficacy, and correlation between parameters were determined.

Results The MTRasym(3.5 ppm) and D_{app} values of the adenocarcinoma (CA) group were higher than those of the cervical squamous carcinoma (CSC) group, while the K_{app} values were lower than those of the CSC group. The MTRasym(3.5 ppm) and K_{app} values of the high-grade group were higher than those of the low-grade group, while the D_{app} values were lower than those of the low-grade group. The D_{app} values of the advanced-stage group were lower than those of the early-stage group, while the K_{app} values were greater than those of the early-stage group. The K_{app} showed the highest efficacy in differentiating CSC and CA, high- and low-grade CC, and advanced- and early-stage CC. In the CSC and CA groups, both the K_{app} and D_{app} were highly correlated with pathological grade, and the MTRasym(3.5 ppm) was weakly correlated with pathological grade. The K_{app}, D_{app}, and MTRasym(3.5 ppm) were all weakly correlated with pathological stage.

Conclusion Both DKI and APTWI can be used in preliminary evaluations of CC, but DKI has advantages in the identification of pathological type, grade, and stage.

Key Points
• *PTWI and DKI provide new information regarding cervical cancer.*
• *MTRasym(3.5 ppm), D_{app}, and K_{app} are valid parameters to characterize tissue microstructure.*
• *DKI is superior to APTWI in the study of cervical cancer.*

Keywords Cervical cancer · Amide proton transfer-weighted imaging · Diffusion kurtosis imaging

---

Nan Meng and Xuejia Wang contributed equally to this work and should be considered co-first authors.

✉ Meiyun Wang
mywang@ha.edu.cn

1. Department of Radiology, Zhengzhou University People's Hospital & Henan Provincial People's Hospital, Zhengzhou, Henan, China

2. Academy of Medical Sciences, Zhengzhou University, Zhengzhou, Henan, China

3. Department of MR, the First Affiliated Hospital, Xinxiang Medical University, Weihui, China

4. Department of Pediatrics, Zhengzhou Central Hospital, Zhengzhou University, Zhengzhou, China

5. MR Research China, GE Healthcare, Beijing, China

Abbreviations

APTWI	Amide proton transfer-weighted imaging
AUC	Area under the curve
CA	Cervical adenocarcinoma
CC	Cervical cancer
CSC	Cervical squamous carcinoma
D_{app}	Mean diffusivity
DKI	Diffusion kurtosis imaging
FIGO	International Federation of Gynecology and Obstetrics
ICC	Intraclass correlation coefficient
K_{app}	Mean kurtosis
MRI	Magnetic resonance imaging
MTRasym (3.5 ppm)	The asymmetric magnetization transfer ratio at 3.5 ppm

RF   Radio frequency
ROC   Receiver operating characteristic
ROI   Region of interest

Introduction

Cervical cancer (CC) is the fourth most prevalent cancer in women worldwide after breast cancer, colorectal cancer, and lung cancer [1]. In developing countries and regions, the incidence of CC is increasing annually, and the affected population is becoming increasingly younger [2]. Among the numerous factors that affect CC treatment and prognosis, the pathological type [3–5], grade, and stage [6, 7] of CC are important. Histopathological results are currently used as the gold standard in clinical practice to determine the stage, type, and grade of CC. However, due to the influence of multiple factors, such as lesion size, tumor heterogeneity, and operator experience, potential risks caused by sampling errors are unavoidable during either surgical resection of gross specimens or stereotactic aspiration within a small area [8, 9].

Magnetic resonance imaging (MRI) is currently the preferred imaging method for CC evaluation and staging. However, conventional sequences can only reflect macroscopic information, such as the lesion location, size, and invasion depth, but cannot effectively evaluate microscopic information, such as the pathological type and grade of diseased tissue. Diffusion kurtosis imaging (DKI) was first proposed by Jenson et al [10] in 2005. DKI is a new diffusion imaging technique based on the theory of a non-Gaussian distribution of water molecules in tissues. DKI fully considers the complexity of the diffusion motion of water molecules inside tissues and introduces fourth-order 3-dimensional tensors based on the original diffusion imaging model; this allows a more accurate quantitative analysis of the diffusion characteristics of water molecules in tissues and thus reflects the complexity of the microstructure of tissues with high sensitivity [11]. Many studies have shown that DKI has considerable potential in the evaluation of stroke [12], grading of gliomas [13], and diagnostic assessment of breast [14] and prostate [15] lesions. In contrast to DKI, amide proton transfer-weighted imaging (APTWI) does not rely on the detection of the diffusion of water molecules in tissues to obtain lesion information, but rather reflects the characteristics of lesions by detecting the content of free proteins and polypeptides in tissues [16]. The basic principle of APTWI is to use a specific radio frequency (RF) pulse to saturate the amide protons in the free proteins/polypeptides in the tissue and then use the chemical exchange between amide protons and water protons to convert the observed change in amide proton concentration, which are difficult to detect, into changes in water signal that are detectable. This results in the indirect measurement of the contents of free proteins and polypeptides in tissues without the use of exogenous contrast

agents [17]. APTWI has been recognized as a promising molecular imaging method that has been applied in the diagnosis [18], identification [19], and prognostic evaluation [20] of central nervous system diseases and is increasingly used in the diagnosis and identification of diseases, such as lung cancer [21], breast cancer [22], and prostate cancer [23].

At present, relevant studies that have assessed the histological characteristics of CC using APTWI and DKI are still in the early stages [24, 25]. This study aimed to explore the role of APTWI and DKI in differentiating the pathological type, grade, and stage of CC and to provide new insights for the clinical diagnosis and prognostic assessment of CC.

Materials and methods

Study subjects

This study was approved by the ethics committee of our institution. All patients signed informed consent forms before the scans were performed. In all, 176 female patients with cervical lesions who underwent MRI at our hospital between June 2017 and July 2019 were enrolled. Of these, 64 patients were excluded due to incomplete scan sequences or poor image quality that did not meet the diagnostic requirements, treatment with radiotherapy and chemotherapy before scanning, unclear pathological results after scanning, the absence of cervical neoplasms, and the presence of rare cervical malignancies, such as adenosquamous carcinoma. Eventually, 112 subjects were included in this study. According to the 2009 International Federation of Gynecology and Obstetrics (FIGO) staging system and histopathology results, the subjects were divided into a cervical squamous carcinoma (CSC) group, an adenocarcinoma (CA) group, an early-stage group ($< II_B$), and an advanced-stage group ($\geq II_B$). The patients in the CSC and CA groups were divided into a high-grade group (G3) and a low-grade group (G1 + G2) (Fig. 1).

Examination method

A 3.0-T MR scanner (Discovery MR750, GE Healthcare) and a 16-channel phased-array coil were used to scan the pelvis of each patient, ranging from the pubic symphysis to the anterior superior iliac spine. Before scanning, vaginal packing with a gelatin sponge was performed, and the bladder was properly inflated to ensure the proper position of the uterus, which is conducive to the imaging of lesions. First, conventional sequence scans were performed, which included T1WI, T2WI, and DWI [26]. After conventional sequence scanning was completed, under the guidance of an experienced radiologist, the APTWI and DKI [27] sequences were scanned for all

Fig. 1 Flow diagram of the patient selection process

Image processing and analysis
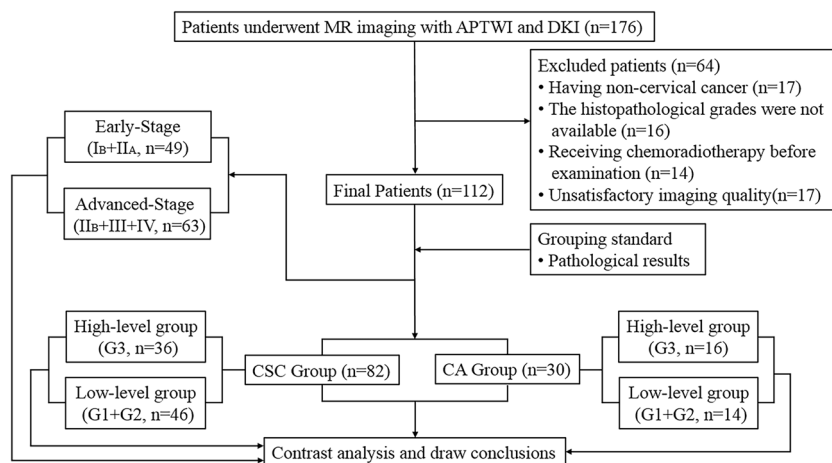
slices containing tumor tissues using the conventional sequence images as references. During the 24 h prior to APTWI scanning, patients did not receive any form of enhanced examination to avoid interference with the APTWI signal [28]. The protocol details are shown in Table 1.

Image processing and analysis

APTWI and DKI images were uploaded to the workstation (Advantage Workstation 4.6, GE Healthcare) and processed and analyzed using relevant software in the Functool toolkit. The first step was to determine the sizes of the tumors based on the T2WI images: tumor volume = the sum of the tumor area of each slice × (slice thickness + interslice gap). The second step was to delineate the regions of interest (ROIs). First, the contours of the solid parts of the tumor tissue were determined on the DWI images using the axial T1WI and T2WI images as references. Subsequently, the pseudo-color images of the APTWI and DKI parameters were merged with the DWI images, and the ROIs were delineated according to the requirements of including the solid parts of the tumor and avoiding large blood vessels, calcification, cystic changes, and hemorrhage as much as possible. The third step was to determine the parameter values. The APTWI parameter was calculated using the equation MTRasym(3.5 ppm) = $[S_{sat}(-3.5\ ppm) - S_{sat}(+3.5\ ppm)]/S_0$, where MTRasym(3.5 ppm) is the asymmetric magnetization transfer ratio (MTR) at 3.5 ppm, S_{sat} is the signal strength after applying the saturation pulse, and S_0 is the signal strength without the saturation pulse. The DKI parameter value was calculated as $S_b = S_0 \times exp.(-b \times D_{app} + b^2 \times D_{app}^2 \times K_{app}/6)$, where S_b represents the signal strength under different b values, D_{app} represents the non-Gaussian diffusion coefficient, and K_{app} represents the apparent kurtosis coefficient. The final value of each tumor parameter was the average of the values of the corresponding tumor parameter in different slices. All of the aforementioned data were independently obtained by 2 experienced radiologists who were blinded to the pathology results.

Statistical methods

The data were analyzed using the statistical software SPSS 23.0 (IBM) and MedCalc 15.0 (MedCalc Software). The intraclass correlation coefficient (ICC) was used to assess interobserver reliability. The Kolmogorov-Smirnov test was used to assess whether the measurement data followed a normal distribution. Differences between different groups were compared using the independent-sample t test and chi-square test. The diagnostic efficacy of each parameter was evaluated using the receiver operating characteristic (ROC) curve, and differences between the area under the curve (AUC) of each parameter were analyzed using the Delong test. Spearman's correlation coefficient was used to analyze the correlation between each parameter and the CC pathological grade. $P < 0.05$ was considered statistically significant.

Results

Study subjects and lesion characteristics

The clinical and pathological characteristics of all the patients are shown in Table 2.

Interobserver reliability

The data measured by the two observers have good consistency (Table 3). Therefore, the averages of the parameter values obtained by the two observers were used as the final evaluation indices.

Comparison of the parameters

The MTRasym(3.5 ppm) and D_{app} values of the CSC group were lower than those of the CA group, and the K_{app} values of the CSC group were greater than those of the CA group. The

Table 1 Imaging protocol parameters

Parameters	T1WI	T2WI	DWI	DKI	APTWI
Sequence	FSE	FSE	SS-EPI	SS-EPI	EPI
Orientation	Axial	Axial	Axial	Axial	Axial
TR/TE (ms)	605/8	5455/109	6000/60.5	2500/58.9	3000/12
FOV (cm^2)	36×36	36×36	36×36	36×36	36×36
Matrix	320×224	320×224	128×128	128×128	128×128
Slice thickness	5	5	5	5	5
NEX	1	1	1, 4	2	1
Bandwidth (Hz/pixel)	62.50	83.33	250	250	250
b-values (s/mm²)	-	-	0, 1000	0, 500, 1000, 1500, 2000	-
Saturation pulse/time	-	-	-	-	2.0 µT, 500 ms
Scan time	1 min 57 s	1 min 33 s	1 min 24 s	5 min 28 s	2 min 36 s (single layer)
Frequency list (only APTWI)	5000, 5000, 5000, ± 600, ± 575, ± 550, ± 525, ± 500, ± 475, ± 450, ± 425, ± 400, ± 375, ± 350, ± 325, ± 300, ± 275, ± 250, ± 225, ± 200, ± 175, ± 150, ± 125, ± 100, ± 75, ± 50, ± 25 Hz (52 frequencies in total)				

FSE fast spin echo, *SS-EPI* single-shot echo planar imaging, *TR/TE* repetition time/echo time, *FOV* field of view, *NEX* number of excitations

MTRasym(3.5 ppm) and D_{app} values of the high-grade CSC and CA groups were lower than those of the low-grade CSC and CA groups, and the K_{app} values of the high-grade CSC and CA groups were greater than those of the low-grade CSC and CA groups. The D_{app} values of the advanced-stage group were lower than those of the early-stage group, and the K_{app} values of the advanced-stage group were greater than those of the early-stage group (Figs. 2, 3, 4; Tables 2, 4).

Comparison of ROC curves

In terms of identifying CSC and CA, AUC (K_{app}) > AUC (D_{app}) > AUC (MTRasym), and the differences between the AUC (K_{app}) and AUC (MTRasym) were statistically significant ($p = 0.046$). In terms of identifying the high-grade and low-grade CSC groups, AUC (K_{app}) > AUC (D_{app}) > AUC (MTRasym), and the difference between the AUC (K_{app}) and AUC (MTRasym) was statistically significant ($p = 0.049$). In terms of identifying the high-grade and low-grade CA groups, AUC (K_{app}) > AUC (D_{app}) > AUC (MTRasym), and the differences between the AUC (K_{app}) and AUC (MTRasym) and between the AUC (D_{app}) and AUC (MTRasym) were statistically significant ($p = 0.046$, 0.047). In terms of identifying the advanced-stage and early-stage groups, AUC (K_{app}) > AUC (D_{app}), but the difference between them was not statistically significant ($p = 0.353$) (Fig. 5, Table 5).

Correlation analysis

In both the CSC and CA groups, the K_{app} had a strong positive correlation with the pathological grade ($r = 0.814$, 0.752, $p < 0.01$), the MTRasym(3.5 ppm) had a mild to moderate positive correlation with the pathological grade ($r = 0.579$, 0.476, $p < 0.01$), and the D_{app} had a strong negative correlation with the pathological grade ($r = -0.720$, -0.728, $p < 0.01$). The K_{app}, D_{app}, and MTRasym(3.5 ppm) values all demonstrate a weak correlation with FIGO stage ($r = 0.436$, -0.358, and 0.198, $p < 0.05$) (Fig. 5).

Discussion

Application of APTWI for the study of CC

When the use of APTWI was compared in the CSC and the CA groups, we found that the MTRasym(3.5 ppm) values of the CSC group were significantly lower than those of the CA group, which is similar to the findings of Ohno et al [21], indicating that compared with CSC, CA has a faster amide proton-free water exchange rate per unit volume of tissue. Three possible causes may account for this phenomenon. The first possible cause is the difference in the protein secretion capacity of cells. The CA originates from endocervical cells and is therefore rich in glandular structures and has the ability to secrete mucins. The CSC originates from cervical epithelial cells and therefore lacks glandular structures and the ability to secrete mucins. The second possible cause is the difference in microvessel density (MVD) in tissues. Zheng et al [29] found that due to the high protein and polypeptide contents, blood in tumor blood vessels is a potential source of hyperintense signals seen on APTWI. The tissue structure of CA is loose, which is conducive to blood vessel growth. Therefore, the MVD of CA is significantly greater than that of CSC [30]. The third possible cause is the different pH values of the 2 microenvironments. Whether the pH values

Table 2 Characteristics of patients and lesions

Characteristics	CA (n = 30)	CSC (n = 82)	p value	High CSC (n = 36)	Low CSC (n = 46)	p value	High CA (n = 16)	Low CA (n = 14)	p value
Patient characteristic									
Age (years)	60.47 ± 9.41	59.84 ± 8.47	0.738	59.33 ± 7.59	60.24 ± 9.16	0.634	60.06 ± 9.72	60.93 ± 9.38	0.806
Menstrual status			0.968			0.250			0.818
Premenopausal	10 (30)	27 (82)		11 (36)	9 (46)		4 (16)	3 (14)	
Postmenopausal	20 (30)	55 (82)		25 (36)	37 (46)		12 (16)	11 (14)	
Lesion characteristic									
Volume (cm^3)	51.92 ± 15.61	46.43 ± 19.52	0.002	45.91 ± 21.42	46.43 ± 19.52	0.002	53.13 ± 16.32	50.53 ± 15.22	0.002
Cystic and necrotic	7 (30)	26 (82)	0.389	20 (36)	6 (46)	<0.001	6 (16)	1 (14)	0.086
Calcifications	1 (30)	3 (82)	0.935	3 (36)	0 (46)	0.161	1 (16)	0 (14)	0.533
Hemorrhagic areas	7 (30)	13 (82)	0.360	11 (36)	2 (46)	0.001	4 (16)	3 (14)	0.581
Vascular shadows	3 (30)	4 (82)	0.582	3 (36)	1 (46)	0.442	2 (16)	1 (14)	0.552
FIGO stage			0.361			<0.001			0.156
Early stage (IB + II$_A$)	4 + 7 (30)	18 + 20 (82)		1 + 6 (36)	14 + 17 (46)		2 + 2 (16)	3 + 4 (14)	
Advanced stage (II$_B$ + III + IV)	7 + 6 + 6 (30)	15 + 16 + 13 (82)		10 + 10 + 9 (36)	5 + 6 + 4 (46)		3 + 5 + 4 (16)	4 + 2 + 1 (14)	
Parameters									
K_{app} value	0.74 ± 0.06	0.88 ± 0.09	<0.001	0.95 ± 0.04	0.83 ± 0.08	<0.001	0.77 ± 0.06	0.71 ± 0.03	0.003
D_{app} value ($\times 10^{-3}$ mm^2/s)	1.11 ± 0.09	0.96 ± 0.12	<0.001	0.88 ± 0.09	1.02 ± 0.10	<0.001	1.06 ± 0.07	1.17 ± 0.06	<0.001
MTRasym(3.5 ppm) value (%)	3.36 ± 0.45	2.89 ± 0.51	<0.001	3.21 ± 0.48	2.64 ± 0.36	<0.001	3.51 ± 0.48	3.19 ± 0.35	0.04

CSC cervical squamous carcinoma, *CA* cervical adenocarcinoma

of CSC and CA tissues are different remains unclear, but local pH changes may occur in CSC, since the microenvironment tends to be in an anoxic state due to the tumor characteristics of high cell density and few blood vessels, affecting the rate of exchange between amide protons and water protons.

This study also found that the MTRasym(3.5 ppm) values of the high-grade groups were generally higher than those of the low-grade groups for both CSC and CA and that the MTRasym(3.5 ppm) was positively correlated with pathological grade. This result is basically consistent with the findings of Zou et al [31] and Takayama et al [32], indicating that APTWI can allow a preliminary assessment of the pathological grade of CC. The possible causes of this result are discussed below. The first possible cause is the difference in cell density. Because the pathological type is the same, the protein/polypeptide secretion abilities of the cancer cells in the high- and low-grade groups were not significantly different. Higher-grade CC with higher cell density often produces more proteins and polypeptides. The second possible cause is the difference in nuclear atypia. Nuclear atypia has been reported to induce an interaction between the macromolecular substance and the hydrophobic cell membrane, thereby promoting the release of

proteins and polypeptides [33, 34]. Compared with low-grade CC, high-grade CC clearly has more significant nuclear atypia. The third possible cause is the difference in the degree of tissue necrosis. Due to the rapid proliferation of cells and the relative lack of blood supply in high-grade CC, the tissues are prone to necrosis, and the cells release large amounts of proteins and peptides into the surrounding environment with the development of tissue necrosis. Although this study attempted to avoid necrotic areas at the time of ROI delineation, microscopic necrosis in ROIs that could only be identified by microscopy may have increased the APTWI signal intensity [35, 36]. In addition, this study found no significant difference in the MTRasym(3.5 ppm) values between the early-stage and advanced-stage groups. We speculate that this may be related to the insignificant differences in protein and peptide content caused by the abovementioned factors between the early-stage and advanced-groups.

Application of DKI for the study of CC

In this study, the K_{app} values in the CSC group were statistically significantly higher than those in the CA group, and the

Table 3 Interobserver agreement for each parameter of CSC and CA

Parameters	CSC:K_{app}	CSC:D_{app}	CSC:MTRasym(3.5 ppm)	CA:K_{app}	CA:D_{app}	CSC:MTRasym(3.5 ppm)
ICC	0.869	0.842	0.701	0.828	0.815	0.745
95% CI	0.804–0.913	0.766–0.895	0.573–0.796	0.672–0.914	0.649–0.907	0.533–0.869

CSC cervical squamous carcinoma, *CA* cervical adenocarcinoma, *ICC* intraclass correlation coefficient

**Table 4** Comparison of different parameters between early- and advanced-stage groups

Parameters	K_{app}	D_{app} ($\times 10^{-3}$ mm^2/s)	MTRasym(3.5 ppm) (%)
Early stage ($n = 49$)	0.81 ± 0.09	1.03 ± 0.12	2.93 ± 0.61
Advanced stage ($n = 63$)	0.87 ± 0.11	0.97 ± 0.13	3.07 ± 0.46
t-value	3.503	-2.543	1.313
p value	0.001	0.012	0.192

CSC cervical squamous carcinoma, *CA* cervical adenocarcinoma

D_{app} values in the CSC group were statistically significantly lower than those in the CA group. These results indicated that compared with CA, the diffusion of water molecules in CSC was more restricted, and the degree of deviation from a Gaussian distribution was also higher, possibly because CSC is derived from the squamous epithelial cells of the cervix and has the characteristics of high cell density, poor secretion function, and severe tissue necrosis. High cell density and

Fig. 2 **a–f** Female, 55 years, with staging IV, G3 CSC, $K_{app} = 0.943$, $D_{app} = 0.832 \times 10^{-3}$ mm^2/s, MTRasym(3.5 ppm) = 3.39%; **g–l** female, 66 years, with staging I_B, G2 CA, $K_{app} = 0.721$, $D_{app} = 1.06 \times 10^{-3}$ mm^2/s, MTRasym(3.5 ppm) = 3.16%. In these images, **a/g** are DKI original images, **b/h** are K_{app} pseudo-colored maps, **c/i** are D_{app} pseudo-colored maps, **d/j** are APTWI original images, **e/k** are MTRasym(3.5 ppm) pseudo-colored maps, and **f/l** are pathological images
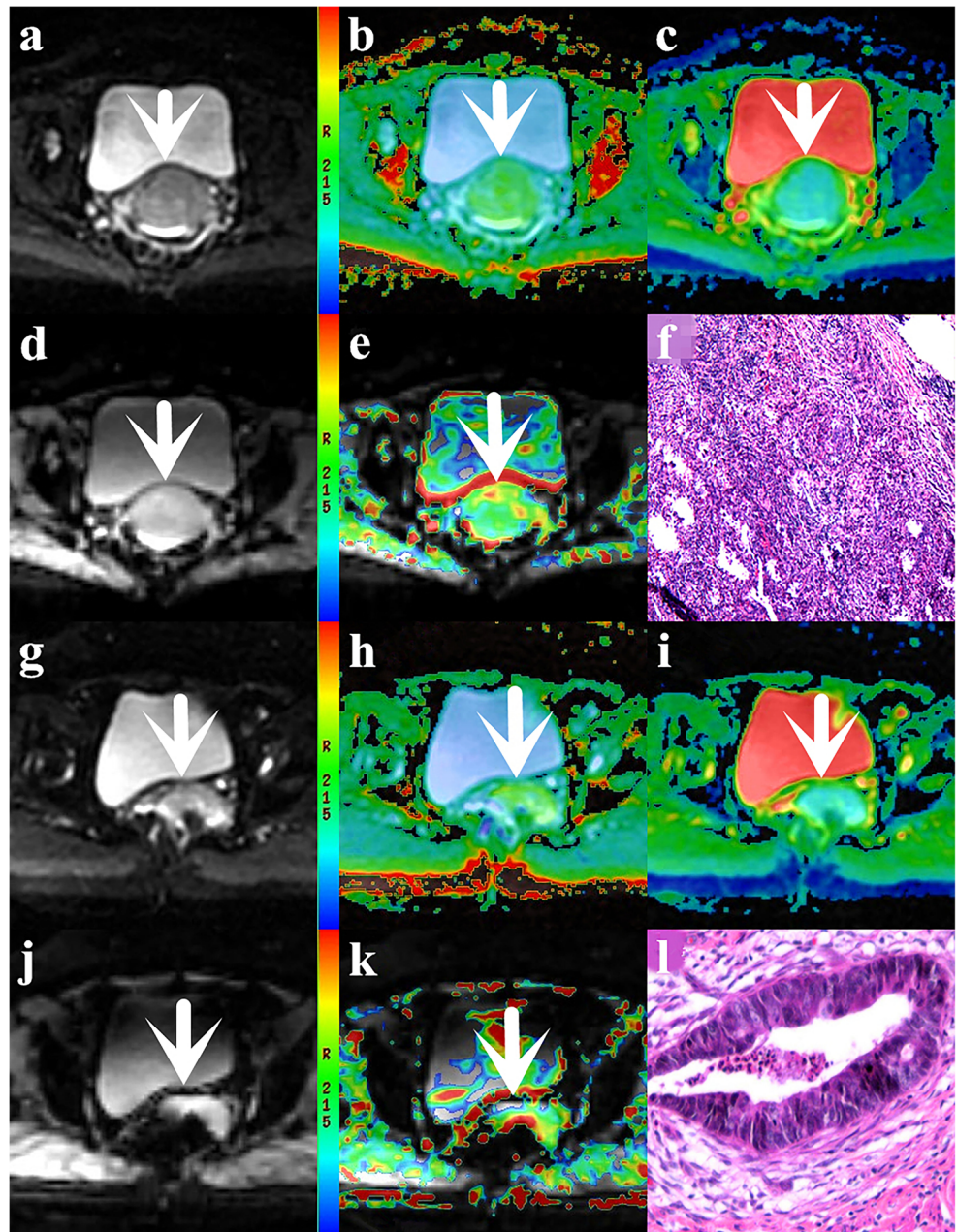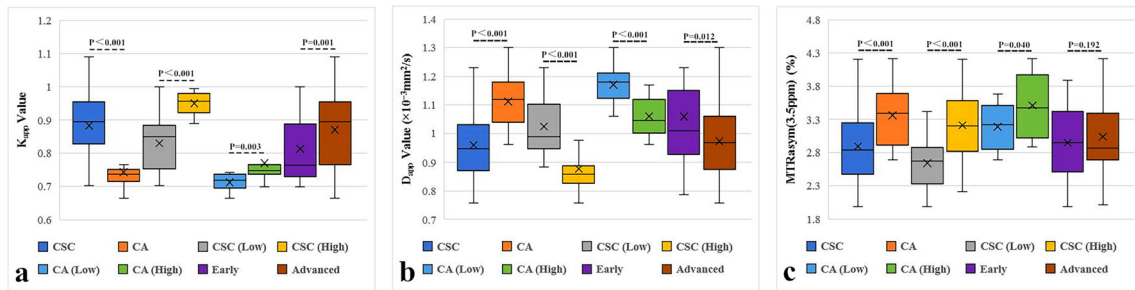
Fig. 3 **a** The box chart for K_{app} values in different groups. **b** The box chart for D_{app} values in different groups. **c** The box chart for MTRasym(3.5 ppm) values in different groups

poor secretion function narrow the gaps between cells and decrease the water content of cells in CSC tissue, which is not conducive to the diffusion of water molecules. Moreover, severe tissue necrosis leads to the complex microscopic structure of CSC tissue and the deviation of the diffusion of water molecules from a Gaussian distribution. In contrast, CA, which originates from endocervical cells, not only has a loose cell structure and strong secretion function but also has less tissue necrosis, which makes the diffusion of water molecules easier and closer to the Gaussian distribution.

This study also found that the differences in K_{app} and D_{app} values between the high- and low-grade groups and between the early- and advanced-stage groups were statistically significant. These results are similar to the findings of Wang et al [24], indicating that DKI has positive value for the preliminary assessment of the pathological grade and stage of CC for the following reasons. Compared with low-grade and early-stage CC, respectively, high-grade and advanced-stage CC often exhibit a more compact tissue structure, more significant cellular atypia, and greater tissue necrosis [37,38]. These features

Fig. 4 **a** The ROC curve for all parameters in the CSC group and the CA group. **b** The ROC curve for all parameters in the high CSC group and low CSC group. **c** The ROC curve for all parameters in the high CA group and low CA group. **d** The ROC curve for all parameters in the advanced-stage group and early-stage group
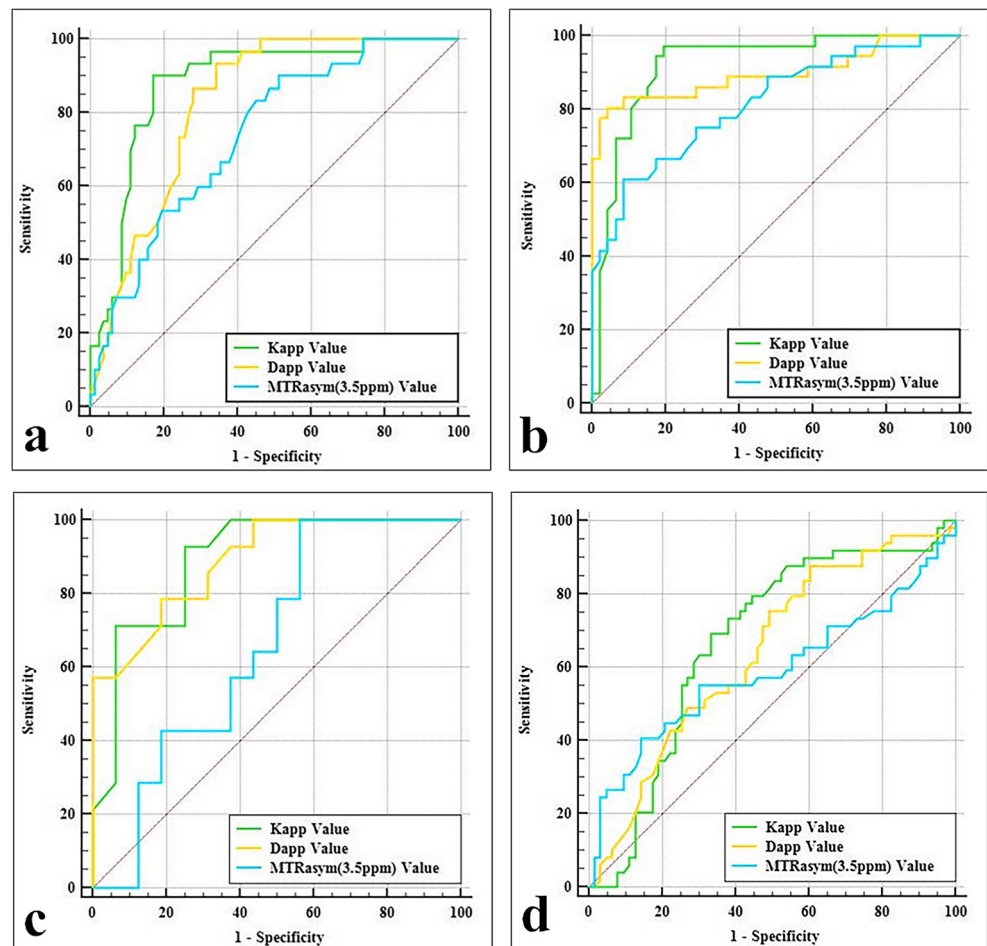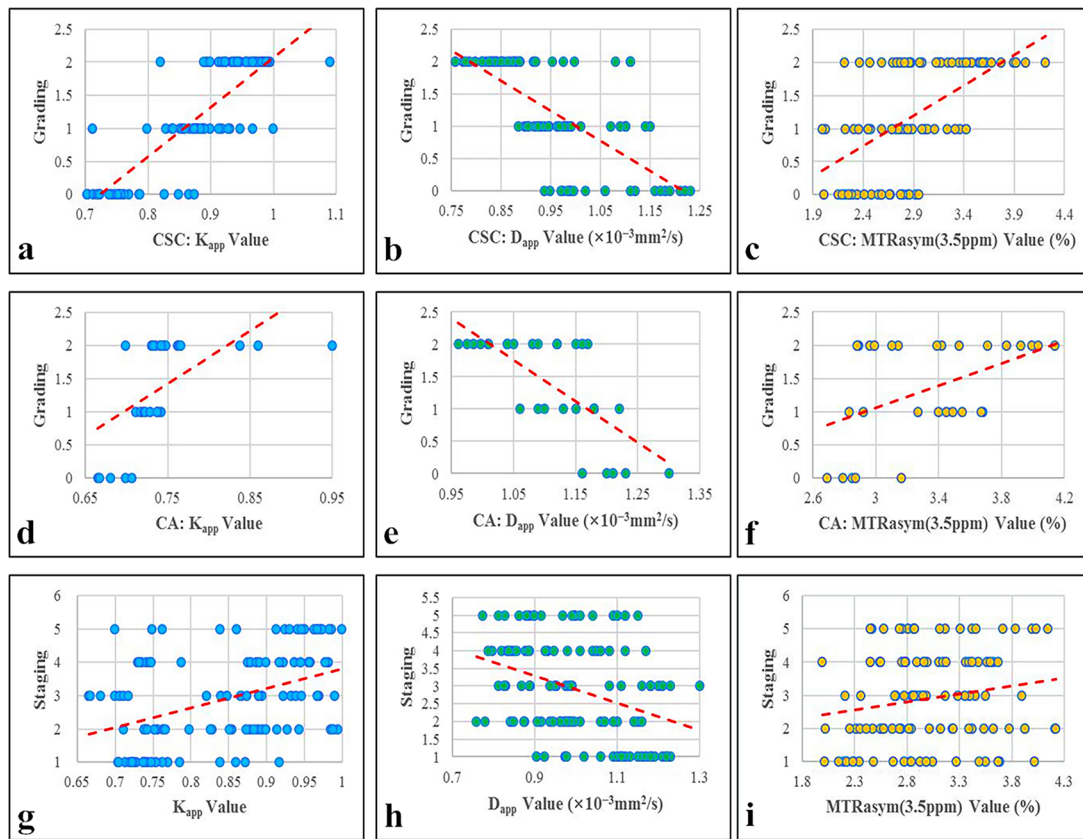
Fig. 5 **a**–**c** The correlation between pathological grading and different parameters (K_{app}, D_{app}, MTRasym(3.5 ppm)) of CSC group ($r = 0.814$, -0.720, 0.579, $p < 0.01$). **d**–**f** The correlation between pathological grading and different parameters of CA group ($r = 0.752$, -0.728, and 0.476, $p < 0.01$). **g**–**i** The correlation between pathological staging and different parameters ($r = 0.436$, -0.358, and 0.198, $p < 0.05$)

Table 5 Comparison of ROC curves for different groups

Parameters	AUC	p value	Threshold	Sensitivity (%)	Specificity (%)	95% CI
CSC vs CA						
K_{app}	0.882	< 0.001	0.766	90.00	82.93	0.808–0.935
D_{app} ($\times 10^{-3}$ mm^2/s)	0.826	< 0.001	0.983	93.33	65.85	0.743–0.891
MTRasym(3.5 ppm) (%)	0.740	< 0.001	2.820	90.00	48.78	0.648–0.818
CSC: high vs low						
K_{app}	0.921	< 0.001	0.888	97.22	80.43	0.840–0.969
D_{app} ($\times 10^{-3}$ mm^2/s)	0.897	< 0.001	0.899	80.56	95.65	0.811–0.953
MTRasym(3.5 ppm) (%)	0.816	< 0.001	3.110	61.11	91.30	0.715–0.893
CA: high vs low						
K_{app}	0.893	< 0.001	0.738	92.86	75.00	0.726–0.976
D_{app} ($\times 10^{-3}$ mm^2/s)	0.891	< 0.001	1.120	78.57	81.25	0.723–0.975
MTRasym(3.5 ppm) (%)	0.661	0.122	3.670	92.86	43.75	0.466–0.822
Early vs advanced						
K_{app}	0.671	0.001	0.859	69.39	66.67	0.576–0.757
D_{app} ($\times 10^{-3}$ mm^2/s)	0.641	0.018	0.899	87.76	39.68	0.545–0.729
MTRasym(3.5 ppm) (%)	0.588	0.125	2.670	40.82	85.71	0.492–0.681

CSC cervical squamous carcinoma, *CA* cervical adenocarcinoma

increase the complexity of the microstructure of diseased tissues and further restrict the diffusion of water molecules, resulting in higher K_{app} values and lower D_{app} values for high-grade and advanced-stage CC compared with those for low-grade and early-stage CC, respectively. In addition, the difference in the mucin secretion ability between the high-grade and low-grade CA groups may have also led to the difference in their DKI values because with an increasing pathological grade, hyperproliferative and dedifferentiated cancer cells may lose their ability to secrete mucin.

Comparative analysis of APTWI and DKI

In our study, DKI has a better diagnostic performance and a higher correlation with pathological grade and stage than APTWI, and the possible reasons for this are discussed below. First, the differences in free protein/polypeptide content between different types of CC are smaller than the differences in the diffusion of water molecules. Second, although various factors affecting the diffusion of water molecules in tissues have been identified, the factors that cause changes in the protein and polypeptide contents in the microenvironment still require further exploration. Third, compared with DKI, APTWI scanning technology and the accuracy of scanning still require improvement.

The limitations of this study are as follows: (1) A single APTWI scan yields only 1 single-slice image; to fully capture the characteristics of lesions, multiple scans must be performed, significantly increasing the scanning time. (2) No unified standard exists for the number and value of b used in DKI scanning, and the repeatability of the b value used in this study requires further verification. (3) The APTWI and DKI sequences used in this study were all developed from the EPI sequence. These sequences have poor resolution and signal-to-noise ratios and are susceptible to various types of artifacts, leading to low-quality images of some small lesions and affecting the accuracy of this experiment to some extent. 4) In this study, cystic changes and necrotic areas were intentionally avoided during ROI delineation, resulting in reduced heterogeneity of the tumor tissues; this may affect the diagnostic efficacy of some parameters. In future work, our team will actively seek solutions to overcome these problems and continue to improve these imaging methods to ensure stable and reliable experimental results.

Conclusion

Both DKI and APTWI can be used to perform preliminary evaluations of CC, but DKI has advantages over APTWI in the identification of pathological type, grade, and stage.

Compliance with ethical standards

Guarantor The scientific guarantor of this publication is Meiyun Wang.

Conflict of interest One of the authors of this manuscript (Kaiyu Wang) is an employee of GE Healthcare. The remaining authors declare no relationships with any companies whose products or services may be related to the subject matter of the article.

Statistics and biometry No complex statistical methods were necessary for this paper.

Informed consent Written informed consent was obtained from all subjects (patients) in this study.

Ethical approval Institutional Review Board approval was obtained.

Study subjects or cohorts overlap Some study subjects or cohorts have been previously reported in *Magnetic Resonance Imaging*.

Methodology
• Prospective
• Diagnostic or prognostic study
• Performed at one institution

References

1. Small W, Bacon MA, Bajaj A et al (2017) Cervical cancer: a global health crisis. Cancer 123:2404–2412
2. Berek JS, Matsuo K, Grubbs BH et al (2019) Multidisciplinary perspectives on newly revised 2018 FIGO staging of cancer of the cervix uteri. J Gynecol Oncol 30:e40
3. Jonska-Gmyrek J, Gmyrek L, Zolciak-Siwinska A, Kowalska M, Kotowicz B (2019) Adenocarcinoma histology is a poor prognostic factor in locally advanced cervical cancer. Curr Med Res Opin 35:595–601
4. Jung EJ, Byun JM, Kim YN et al (2017) Cervical adenocarcinoma has a poorer prognosis and a higher propensity for distant recurrence than squamous cell carcinoma. Int J Gynecol Cancer 27:1228–1236
5. Fujiwara H, Yokota H, Monk B et al (2014) Gynecologic Cancer InterGroup (GCIG) consensus review for cervical adenocarcinoma. Int J Gynecol Cancer 24:S96–S101
6. Pol FJ, Zusterzeel PL, van Ham MA, Kuijpers DA, Bulten J, Massuger LF (2015) Satellite lymphovascular space invasion: an independent risk factor in early stage cervical cancer. Gynecol Oncol 138:579–584
7. Shoji T, Takatori E, Saito T et al (2013) Neoadjuvant chemotherapy using platinum- and taxane-based regimens for bulky stage Ib2 to

IIb non-squamous cell carcinoma of the uterine cervix. Cancer Chemother Pharmacol 71:657–662

8. Kalliala I, Anttila A, Nieminen P, Halttunen M, Dyba T (2014) Pregnancy incidence and outcome before and after cervical intraepithelial neoplasia: a retrospective cohort study. Cancer Med 3:1512–1516

9. Moukarzel LA, Angarita AM, VandenBussche C et al (2017) Preinvasive and invasive cervical adenocarcinoma: preceding low-risk or negative pap result increases time to diagnosis. J Low Genit Tract Dis 21:91–96

10. Jensen JH, Helpern JA, Ramani A, Lu H, Kaczynski K (2005) Diffusional kurtosis imaging: the quantification of non-Gaussian water diffusion by means of magnetic resonance imaging. Magn Reson Med 53:1432–1440

11. Jensen JH, Helpern JA (2010) MRI quantification of non-Gaussian water diffusion by kurtosis analysis. NMR Biomed 23:698–710

12. Yin J, Sun H, Wang Z, Ni H, Shen W, Sun PZ (2018) Diffusion kurtosis imaging of acute infarction: comparison with routine diffusion and follow-up MR imaging. Radiology 287:651–657

13. Hempel JM, Schittenhelm J, Bisdas S et al (2018) In vivo assessment of tumor heterogeneity in WHO 2016 glioma grades using diffusion kurtosis imaging: diagnostic performance and improvement of feasibility in routine clinical practice. J Neuroradiol 45:32–40

14. Sun K, Chen X, Chai W et al (2015) Breast cancer: diffusion kurtosis MR imaging-diagnostic accuracy and correlation with clinical-pathologic factors. Radiology 277:46–55

15. Suo S, Chen X, Wu L et al (2014) Non-Gaussian water diffusion kurtosis imaging of prostate cancer. Magn Reson Imaging 32:421–427

16. Zhou J, Payen JF, Wilson DA, Traystman RJ, van Zijl PC (2003) Using the amide proton signals of intracellular proteins and peptides to detect pH effects in MRI. Nat Med 9:1085–1090

17. Zhou J, Lal B, Wilson DA, Laterra J, van Zijl PC (2003) Amide proton transfer (APT) contrast for imaging of brain tumors. Magn Reson Med 50:1120–1126

18. Jeong HK, Han K, Zhou J et al (2017) Characterizing amide proton transfer imaging in haemorrhage brain lesions using 3T MRI. Eur Radiol 27:1577–1584

19. Joo B, Han K, Choi YS et al (2018) Amide proton transfer imaging for differentiation of benign and atypical meningiomas. Eur Radiol 28:331–339

20. Jiang S, Eberhart CG, Lim M et al (2019) Identifying recurrent malignant glioma after treatment using amide proton transfer-weighted MR imaging: a validation study with image-guided stereotactic biopsy. Clin Cancer Res 25:552–561

21. Ohno Y, Yui M, Koyama H et al (2016) Chemical exchange saturation transfer MR imaging: preliminary results for differentiation of malignant and benign thoracic lesions. Radiology 279:578–589

22. Dula AN, Dewey BE, Arlinghaus LR et al (2015) Optimization of 7-T chemical exchange saturation transfer parameters for validation of glycosaminoglycan and amide proton transfer of fibroglandular breast tissue. Radiology 275:255–261

23. Takayama Y, Nishie A, Sugimoto M et al (2016) Amide proton transfer (APT) magnetic resonance imaging of prostate cancer: comparison with Gleason scores. MAGMA 29:671–679

24. Wang P, Thapa D, Wu G, Sun Q, Cai H, Tuo F (2018) A study on diffusion and kurtosis features of cervical cancer based on non-Gaussian diffusion weighted model. Magn Reson Imaging 47:60–66

25. Li B, Sun H, Zhang S, Wang X, Guo Q (2019) The utility of APT and IVIM in the diagnosis and differentiation of squamous cell carcinoma of the cervix: a pilot study. Magn Reson Imaging 63:105–113

26. Dappa E, Elger T, Hasenburg A, Düber C, Battista MJ, Hötker AM (2017) The value of advanced MRI techniques in the assessment of cervical cancer: a review. Insights Imaging 8:471–481

27. Rosenkrantz AB, Padhani AR, Chenevert TL et al (2015) Body diffusion kurtosis imaging: basic principles, applications, and considerations for clinical practice. J Magn Reson Imaging 42:1190–1202

28. Tee YK, Donahue MJ, Harston GW, Payne SJ, Chappell MA (2014) Quantification of amide proton transfer effect pre- and post-gadolinium contrast agent administration. J Magn Reson Imaging 40:832–838

29. Zheng S, van der Bom IM, Zu Z, Lin G, Zhao Y, Gounis MJ (2014) Chemical exchange saturation transfer effect in blood. Magn Reson Med 71:1082–1092

30. Argüello-Ramírez J, Pérez-Cárdenas E, Delgado-Chávez R, Solorza-Luna G, Villa-Treviño S, Arenas-Huertero F (2004) Matrix metalloproteinases-2, -3, and -9 secreted by explants of benign and malignant lesions of the uterine cervix. Int J Gynecol Cancer 14:333–340

31. Zou T, Yu H, Jiang C et al (2018) Differentiating the histologic grades of gliomas preoperatively using amide proton transfer-weighted (APTW) and intravoxel incoherent motion MRI. NMR Biomed 31:e3850

32. Takayama Y, Nishie A, Togao O et al (2018) Amide proton transfer MR imaging of endometrioid endometrial adenocarcinoma: association with histologic grade. Radiology 286:909–917

33. Tang Y, Dundamadappa SK, Thangasamy S et al (2014) Correlation of apparent diffusion coefficient with Ki-67 proliferation index in grading meningioma. AJR Am J Roentgenol 202:1303–1308

34. Whittaker CS, Coady A, Culver L, Rustin G, Padwick M, Padhani AR (2009) Diffusion-weighted MR imaging of female pelvic tumors: a pictorial review. Radiographics 29:759–774 discussion 774-778

35. Togao O, Yoshiura T, Keupp J et al (2014) Amide proton transfer imaging of adult diffuse gliomas: correlation with histopathological grades. Neuro Oncol 16:441–448

36. Togao O, Hiwatashi A, Yamashita K et al (2017) Grading diffuse gliomas without intense contrast enhancement by amide proton transfer MR imaging: comparisons with diffusion- and perfusion-weighted imaging. Eur Radiol 27:578–588

37. Yue W, Meng N, Wang J et al (2019) Comparative analysis of the value of diffusion kurtosis imaging and diffusion-weighted imaging in evaluating the histological features of endometrial cancer. Cancer Imaging 19:9